Available online at www.sciencedirect.com
ScienceDirect
Icarus 195 (2008) 765–777
ICARUS
www.elsevier.com/locate/icarus

# Astrometry and dynamics of Anthe (S/2007 S 4), a new satellite of Saturn

N.J. Cooper [a,*], C.D. Murray [a], M.W. Evans [a], K. Beurle [a], R.A. Jacobson [b], C.C. Porco [c]

[a] *Astronomy Unit, School of Mathematical Sciences, Queen Mary, University of London, Mile End Road, London E1 4NS, UK*
[b] *Jet Propulsion Laboratory, California Institute of Technology, 4800 Oak Grove Drive, Pasadena, CA 91109-8099, USA*
[c] *Cassini Imaging Central Laboratory for Operations (CICLOPS), Space Science Institute, 4750 Walnut Street, Suite 205, Boulder, CO 80301, USA*

Received 31 October 2007; revised 8 January 2008

Available online 5 February 2008

**Abstract**

We describe the astrometry and dynamics of Anthe (S/2007 S 4), a new satellite of Saturn discovered in images obtained using the Imaging Science Subsystem (ISS) of the *Cassini* spacecraft. Included are details of 63 observations, of which 28 were obtained with *Cassini*'s narrow-angle camera (NAC) and 35 using its wide-angle camera (WAC), covering an observation time-span of approximately 3 years. We estimate the diameter of Anthe to be ∼1.8 km. Orbit modeling based on a numerical integration of the full equations of motion fitted to the observations show that Anthe is in a first-order 11:10 mean motion resonance with Mimas. Two resonant arguments are librating: $\phi_1 = 11\lambda' - 10\lambda - \varpi$ and $\phi_2 = 11\lambda' - 10\lambda - \varpi' - \Omega' + \Omega$, where $\lambda$, $\varpi$ and $\Omega$ refer to the mean longitude, longitude of pericenter and longitude of ascending node of Mimas and Anthe, with the primed quantities corresponding to Anthe. These resonances cause periodic variations in the orbital elements. The semi-major axis varies by ±26 km over a 913-day period. Anthe is also close to a second-order eccentricity-type mean motion resonant relationship of the form 77:75 with Methone. Since Methone is also in a first-order resonance with Mimas [Spitale, J.N., Jacobson, R.A., Porco, C.C., Owen, W.M., 2006. Astron. J. 132, 692–710], an additional indirect perturbation exists between Methone and Anthe via Mimas. Neither effect is detectable in the orbit fitting and the short-term dynamical evolution of Anthe is dominated by the Mimas–Anthe resonances alone. The expected modulation effect from the Mimas–Tethys 4:2 inclination resonance is also insignificant over this time period. By including *Cassini* ISS observations of Mimas in the numerical integration fit, we estimate the $GM$ of Mimas to be $2.509 \pm 0.004$ km$^3$ s$^{-2}$, consistent with Jacobson et al. [Jacobson, R.A., Spitale, J., Porco, C.C., Owen, W.M., 2006. Astron. J. 132, 711–713].


*Keywords:* Satellites, dynamics; Saturn, satellites; Resonances, orbital

## 1. Introduction

Since the start of the approach phase of the *Cassini–Huygens* mission to Saturn in January 2004, *Cassini*'*s* Imaging Science Subsystem (ISS) has been used to make systematic searches for previously unknown saturnian satellites. There have been five discoveries to date. The first discoveries, Methone and Pallene, were found in images taken on 2005 June 1 (Porco et al., 2004a, 2005a). Later that year, Polydeuces, a co-orbital of Dione, was discovered in images taken on 2004 October 21 (Porco et al., 2004b, 2005a; Murray et al., 2005), followed by Daphnis, orbiting within the Keeler Gap in Saturn's A ring, which was located in images from 2005 May 1 (Porco et al., 2005b). Two more years were to pass before the fifth confirmed discovery of a satellite in *Cassini* images, when Anthe, the subject of this current work, was discovered on 2007 June 22 in images taken on 2007 May 30 (Porco et al., 2007).

At the time of the launch of the *Cassini* spacecraft in October 1997, 18 saturnian satellites were known, ranging in physical size from Calypso (radius 9.5 km) to Titan (radius 2575.5 km). In addition to the five new inner satellites discovered by the Cassini ISS, described above, a large number of new irregular satellites have also been discovered using ground-based observations, including most recently S/2007 S 1 (Tarqeq), S/2007 S2 and S/2007 S 3 (Sheppard et al., 2007). The discovery of Anthe, S/2007 S 4 (radius ∼ 0.9 km) has brought the current total number of saturnian satellites to 60.

In this work, we outline the method of discovery of Anthe together with the astrometric data reduction procedures. A table

* Corresponding author. Fax: +44 (0) 20 8983 3522.
*E-mail address:* n.cooper@qmul.ac.uk (N.J. Cooper).

0019-1035/$ – see front matter 
doi:10.1016/j.icarus.2008.01.006

Table 1
Semi-major axes of relevant bodies

| Body | Semi-major axis (km) |
|---|---|
| G-ring | 165,000–176,000[a] |
| Mimas | 185,540 [b] |
| E-ring | 189,870–420,000[a] |
| Methone | 194,230[c] |
| Anthe | 197,655[d] |
| Pallene | 212,280[c] |
| Enceladus | 238,040[b] |
| Tethys | 294,670[b] |
| Dione | 377,420[b] |
| Polydeuces | 377,200[c] |

[a] JPL SPICE kernel cpck17May2007.tpc.
[b] http://ssd.jpl.nasa.gov/.
[c] Jacobson et al. (2007).
[d] This work (mean value, Table 7).

of the reduced observations is included. We describe the orbit modeling method, and then analyze the short-term dynamical evolution of Anthe.

Spitale et al. (2006) showed that Methone is in a 15:14 outer mean motion resonance with Mimas and that Pallene is in an inner 19:16 mean motion resonance with Enceladus. In this work, we show that Anthe is in an unusual first-order mean motion resonance with Mimas, involving both the eccentricities and inclinations. Anthe is the first planetary satellite in the Solar System to be found to occupy a mixed resonance of the kind described. We also identify a possible second-order mean motion resonant relationship between Anthe and Methone. We estimate the mass of Mimas from an analysis of its resonant interaction with Anthe, obtaining a value consistent with Jacobson et al. (2006), who derived their estimate from an analysis of Mimas's resonant interactions with Tethys and Methone.

In Table 1 we provide estimated semi-major axes for the satellites and rings relevant to this work.

## 2. Satellite astrometry

To date, satellites have been discovered in *Cassini* images using three different methods. Methone and Pallene, the first discoveries, were located using an automated search technique. In this procedure, satellite candidate objects were first identified in each image and then cross-correlated with candidate objects in other images (Charnoz, private communication). In the case of Daphnis, discovered orbiting in the Keeler Gap in Saturn's A-ring, the satellite was immediately apparent in the discovery image sequence. The existence of a satellite orbiting in this region had long been suspected after Voyager images had shown the characteristic signature of a satellite, in the form of waves in the edges of the Keeler Gap (Cooke, 1991). The Daphnis discovery sequence, a high resolution 'ansa-stare' movie, had consequently been designed with this in mind. Finally, Polydeuces was discovered by visual inspection of pairs of images using a blink comparison technique, searching for objects whose position changes with respect to the background stars (Murray et al., 2005).

### 2.1. Discovery

Anthe, the subject of this work, was discovered using the same blink comparison technique and software used in the discovery of Polydeuces. These procedures are described in more detail by Murray et al. (2005). As before, where possible, the image positions of Anthe were measured using an IDL (ITT Visual Information Solutions, Boulder, Colorado) application of the DAOPHOT centroiding technique of Stetson (1987). Otherwise observed positions were chosen to be the center of the brightest pixel. Based on this, we believe a reasonable estimate of the measurement uncertainty for each observation is 0.5 pixel. Camera pointing corrections for each image were once again determined using IDL-based procedures within the framework of the CAVIAR package developed at Queen Mary, University of London (Murray et al., 2005). For the observations of Anthe described here, the typical rms residual for the stars in a pointed image was better than 0.1 pixel (equivalent to 0.12357 arcsec for the NAC images and 1.2324 arcsec for the WAC images).

Anthe was discovered on 2007 June 22, using blink comparison between WAC images W1559190974 and W1559191022. This image pair was taken on 2007 May 30, with a time separation of 50.5 s. During that time, Anthe had moved by ∼1.6 pixels between images with respect to the background stars. In the next image pair, W1559193373 and W1559193421, again taken 50.5 s apart, Anthe had moved by ∼1.8 pixels between the pair of images. These two image pairs are separated by 39 min 59 s (time between the first images in each pair) and Anthe had moved by ∼33 pixels in this time interval. The third pair of images examined, W1559195773 and W1559195821, also showed Anthe moving against the background stars. All six of these images suggested an object orbiting at a radial distance from Saturn of ∼197,700 km, based on the calculated ring plane intercepts of the line of sight vectors from the *Cassini* spacecraft to the object locations in the images. Such an object would be orbiting exterior to Mimas and Methone, but interior to Pallene. By the end of the day on June 22 the number of images in which Anthe had been detected had risen to 24 (12 pairs), all from the observation ISS_045RE_LPMRDFMOV001_PRIME, executed on 2007 May 30. The discovery image pair is shown in Fig. 1.

### 2.2. Preliminary orbit

Up to this point, since all the images were part of the same observation and shuttered sequentially, with image pairs taken every ∼20 min, an initial orbit fit had not been necessary to generate a list of images and line, sample predicted locations within those images, to search for further detections. Nevertheless an initial orbit solution with an rms residual of 2.74 WAC pixels had been determined as soon as the first 4 detections were available, based on a precessing ellipse model. This initial orbit fit was sufficient to confirm that the detected object was moving in a Keplerian orbit between Methone and Pallene. This orbit was updated as more detections became available so that by the end of June 22, the fit residuals had reduced to 0.32 WAC pixels.

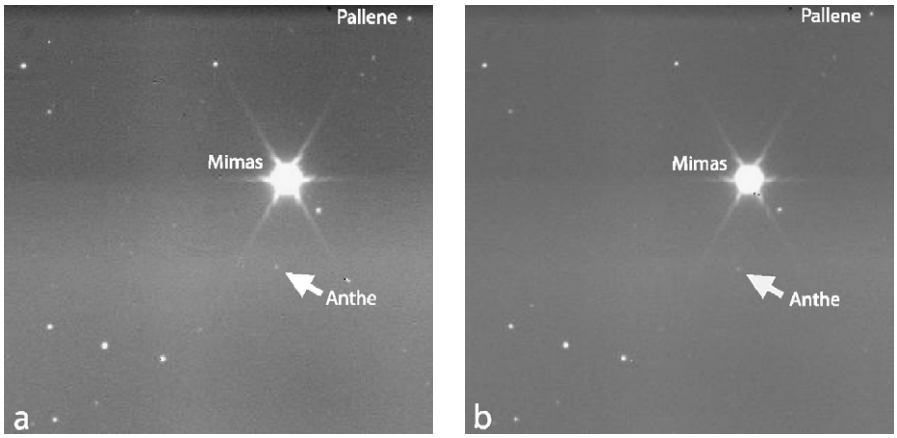


Fig. 1. Sections of the two discovery images (a) W1559190974 and (b) W1559191022. The left-hand image was recorded at 2007 May 30 04:02:02.511 with an exposure duration of 15 s and the right-hand image 55.507 s later, with exposure duration of 10 s. The images have been enhanced to show Anthe. Two other saturnian satellites, Mimas and Pallene, are also present.

### 2.3. Recovery and orbital refinement

On the following day, 2007 June 23, the remaining 6 images in the observation ISS_045RE_LPMRDFMOV001_PRIME that included Anthe were identified using blink comparison, bringing the total number of detections to 30 (those observations dated 2007 May 30 in Table 2). From this point onwards, location of further observations and refinement of the orbit solution proceeded in tandem, the latest orbit fit being used to identify images that were predicted to contain Anthe and then the images themselves being examined. In this way 5 more images, those taken on 2007 May 31 (Table 2), were identified on June 23, bringing the total number of detections to 35 spanning just under 30 h (equivalent to approximately 1.2 orbits).

At the earliest possible opportunity, an attempt was made to fit a numerical integration of the full equations of motion to the available observations, to provide an orbit solution which would take into account possible gravitational perturbations from other satellites. The first integrated solution was produced on 2007 June 24 using 21 WAC observations spanning 30 h with an rms uncertainty in the position vector of Anthe of 104.9 km. An analysis of the orbital elements from a 10-year forward integration of this orbit revealed a significant resonant effect, implying that a 2-body precessing ellipse orbit solution would be inadequate for the tracking and possible recovery of Anthe in earlier images. As of 2007 June 25, 3 days after discovery, an orbital integration was used for search purposes. The orbital analysis and dynamical evolution of Anthe are discussed in more detail in Sections 3 and 4.

An important breakthrough came on 2000 June 25, with the re-examination of an image pair from the ISS_000RI_SATSRCHBP003_PRIME observation, taken 3 years previously on 2004 June 1, in which the satellites Methone and Pallene had previously been discovered. Around the time of the Methone and Pallene discovery, a note had been made of an additional possible candidate satellite detection in the image pair N1464780112 and N1464780153. This candidate had yet to be identified. However, when checking against the initial integrated orbit for Anthe, the predicted position of Anthe was found to be within 5 or 6 pixels of the unidentified object, despite the 3-year time gap. Using 4 detections from this sequence, the orbital integration was revised, halving the rms uncertainty in the position vector for Anthe to 49.6 km. In all 6 detections from this sequence are included in Table 2, all of which were located independently of any orbital prediction. Although other candidate detections of Anthe were subsequently located in this image sequence, based on the orbit prediction, most were only 1–3 DN brighter than the local background. Because these detections were so borderline, we could not be sufficiently confident that they were genuine detections of the same object seen in the images from 2007 May 30 and 31. The very faintness of Anthe in these images also probably explains why it was not discovered by the automatic batch processing software at the same time as Methone and Pallene (Charnoz, private communication; Porco et al., 2005a). By 2007 June 25, 41 detections of Anthe had been made.

Four days after discovery, 2007 June 26, saw the identification of an image of Anthe that brought further significant reduction in the size of the uncertainties in the orbit solution. The examination of *Cassini* ISS images for new satellites had been ongoing since January 2004 with the start of the Approach Science Phase of the *Cassini* mission. On 2005 February 17, it had been noted that the image N1475699034, taken on 2004 October 5, contained an unusual trail, with a predicted ring plane radial location of 197,418 km, and with an orientation different from the star trails in the same image. At the time this was not pursued further as there were no other satellite candidate detections that had a corresponding ring plane radial distance. Since the existing fit for Anthe gave a semi-major axis of 197,669 km, the image was examined again and the predicted location of Anthe found to be only ∼7 pixels from one end of the trail. This brought the number of detections of Anthe to 42 with an observed arc of 967 days. A revised orbit solution was obtained, with the rms uncertainty in the position vector reduced to 16.3 km. The new orbit solution showed the predicted location of Anthe to be coincident with one end of the trail at the time the shutter opened, to take N1475699034, and coincident with the opposite end of the trail when the shutter closed,

Table 2
Cassini ISS observations of Anthe

| Frame | Image mid-time (UTC) | Line[a,b] | Sample | RA[c] (deg) | DEC (deg) |
|---|---|---|---|---|---|
| N1464775792 | 2004 Jun 01 09:45:51.721 | 354.50 | 583.00 | 37.81532 | 9.90357 |
| N1464775833 | 2004 Jun 01 09:46:32.721 | 355.00 | 585.00 | 37.81511 | 9.90428 |
| N1464777232 | 2004 Jun 01 10:09:51.712 | 382.00 | 641.00 | 37.80679 | 9.92312 |
| N1464777273 | 2004 Jun 01 10:10:32.712 | 383.00 | 642.00 | 37.80650 | 9.92370 |
| N1464780112 | 2004 Jun 01 10:57:51.693 | 497.00 | 750.00 | 37.76901 | 9.96091 |
| N1464780153 | 2004 Jun 01 10:58:32.693 | 499.30 | 751.30 | 37.76826 | 9.96149 |
| N1473631252 | 2004 Sep 11 21:32:06.346 | 380.00 | 241.00 | 26.17373 | 10.24891 |
| N1475699034 | 2004 Oct 05 19:56:54.839 | 647.00 | 689.00 | 38.68849 | 8.63143 |
| N1485806755 | 2005 Jan 30 19:39:39.689 | 803.50 | 34.00 | 44.66613 | −2.33171 |
| N1486682596 | 2005 Feb 09 22:56:54.986 | 985.00 | 237.00 | 60.14714 | −3.27546 |
| N1486819667 | 2005 Feb 11 13:01:25.094 | 87.97 | 693.17 | 71.56646 | −2.83280 |
| N1487603917 | 2005 Feb 20 14:52:09.988 | 1009.08 | 473.97 | 40.65141 | −6.59763 |
| N1487966919 | 2005 Feb 24 19:42:09.624 | 734.83 | 457.86 | 55.00721 | −6.28655 |
| N1488234697 | 2005 Feb 27 22:05:06.280 | 247.00 | 372.00 | 63.15907 | −5.93715 |
| N1489384323 | 2005 Mar 13 05:25:24.707 | 34.00 | 489.00 | 39.28160 | −6.48139 |
| N1495629609 | 2005 May 24 12:12:34.902 | 1013.50 | 850.50 | 27.62808 | −2.51722 |
| N1506005825 | 2005 Sep 21 14:28:40.307 | 952.00 | 647.00 | 79.34800 | −4.69158 |
| N1507076645 | 2005 Oct 03 23:55:33.056 | 75.00 | 186.00 | 55.74684 | −5.92493 |
| N1507076735 | 2005 Oct 03 23:57:03.040 | 74.00 | 245.00 | 55.72576 | −5.92545 |
| N1507100106 | 2005 Oct 04 06:26:33.906 | 695.00 | 437.00 | 56.05458 | −5.95153 |
| N1507100196 | 2005 Oct 04 06:28:03.890 | 696.00 | 374.50 | 56.07634 | −5.95110 |
| N1508159988 | 2005 Oct 16 12:51:09.545 | 379.50 | 877.00 | 35.19351 | −6.09191 |
| N1512964624 | 2005 Dec 11 03:27:54.848 | 98.00 | 337.00 | 44.62116 | −6.28079 |
| N1513055615 | 2005 Dec 12 04:44:25.267 | 570.00 | 253.00 | 46.66939 | −6.24574 |
| N1519143588 | 2006 Feb 20 15:49:57.409 | 230.30 | 284.00 | 59.26288 | −5.89241 |
| N1521019196 | 2006 Mar 14 08:49:54.477 | 150.00 | 525.00 | 27.24819 | −6.25392 |
| N1524643223 | 2006 Apr 25 07:29:58.302 | 265.50 | 176.50 | 28.08687 | −6.24037 |
| W1559182574 | 2007 May 30 01:42:02.564 | 119.00 | 431.00 | 189.31136 | 2.30929 |
| W1559182622 | 2007 May 30 01:42:53.071 | 124.00 | 431.50 | 189.33315 | 2.30728 |
| W1559184974 | 2007 May 30 02:22:02.549 | 307.00 | 445.00 | 190.09419 | 2.25366 |
| W1559185022 | 2007 May 30 02:22:53.056 | 310.00 | 445.00 | 190.10859 | 2.25259 |
| W1559186174 | 2007 May 30 02:42:02.541 | 26.50 | 453.50 | 190.42887 | 2.21965 |
| W1559186222 | 2007 May 30 02:42:53.048 | 30.00 | 454.00 | 190.44226 | 2.21764 |
| W1559187374 | 2007 May 30 03:02:02.533 | 453.50 | 461.50 | 190.73449 | 2.18030 |
| W1559187422 | 2007 May 30 03:02:53.041 | 456.00 | 462.00 | 190.74755 | 2.17821 |
| W1559189774 | 2007 May 30 03:42:02.518 | 554.50 | 479.00 | 191.21826 | 2.09392 |
| W1559189822 | 2007 May 30 03:42:53.026 | 555.50 | 480.00 | 191.22637 | 2.09031 |
| W1559190974 | 2007 May 30 04:02:02.511 | 231.50 | 490.00 | 191.39589 | 2.04355 |
| W1559191022 | 2007 May 30 04:02:53.018 | 233.00 | 490.50 | 191.40221 | 2.04225 |
| W1559192173 | 2007 May 30 04:22:01.503 | 605.00 | 499.50 | 191.52925 | 1.99044 |
| W1559192221 | 2007 May 30 04:22:52.010 | 605.30 | 500.00 | 191.53441 | 1.98823 |
| W1559193373 | 2007 May 30 04:42:01.495 | 257.50 | 510.00 | 191.61704 | 1.93409 |
| W1559193421 | 2007 May 30 04:42:52.003 | 258.00 | 511.00 | 191.61996 | 1.93036 |
| W1559194573 | 2007 May 30 05:02:01.488 | 602.50 | 521.00 | 191.65814 | 1.87319 |
| W1559194621 | 2007 May 30 05:02:51.995 | 601.20 | 521.80 | 191.65828 | 1.86910 |
| W1559195773 | 2007 May 30 05:22:01.480 | 228.50 | 532.00 | 191.64943 | 1.80830 |
| W1559195821 | 2007 May 30 05:22:51.988 | 227.80 | 532.80 | 191.64818 | 1.80452 |
| W1559196973 | 2007 May 30 05:42:01.473 | 545.00 | 543.50 | 191.59285 | 1.74102 |
| W1559197021 | 2007 May 30 05:42:51.980 | 543.00 | 544.00 | 191.59042 | 1.73746 |
| W1559198173 | 2007 May 30 06:02:01.465 | 142.50 | 555.00 | 191.48650 | 1.67114 |
| W1559198221 | 2007 May 30 06:02:51.972 | 140.30 | 555.20 | 191.48011 | 1.66822 |
| W1559199373 | 2007 May 30 06:22:01.457 | 429.50 | 566.00 | 191.33401 | 1.59877 |
| W1559199421 | 2007 May 30 06:22:51.965 | 426.00 | 566.00 | 191.32631 | 1.59663 |
| W1559201773 | 2007 May 30 07:02:01.442 | 258.00 | 589.00 | 190.88294 | 1.44908 |
| W1559201821 | 2007 May 30 07:02:51.950 | 253.50 | 589.70 | 190.87203 | 1.44499 |
| W1559204172 | 2007 May 30 07:42:00.427 | 34.00 | 610.00 | 190.25085 | 1.29267 |
| W1559204220 | 2007 May 30 07:42:50.934 | 28.50 | 610.00 | 190.23684 | 1.29053 |
| W1559287414 | 2007 May 31 06:49:20.415 | 471.00 | 552.00 | 196.05988 | 0.31685 |
| W1559287484 | 2007 May 31 06:50:35.319 | 235.00 | 276.00 | 196.05596 | 0.31557 |
| W1559288036 | 2007 May 31 06:59:47.327 | 226.00 | 280.00 | 196.02045 | 0.28101 |
| W1559288068 | 2007 May 31 07:00:17.427 | 224.00 | 280.00 | 196.01483 | 0.27962 |

Table 2 (*continued*)

| Frame | Image mid-time (UTC) | Line[a,b] | Sample | RA[c] (deg) | DEC (deg) |
|---|---|---|---|---|---|
| W1559288100 | 2007 May 31 07:00:49.427 | 224.00 | 280.00 | 196.01480 | 0.27897 |
| N1560618365 | 2007 Jun 15 16:31:47.872 | 213.00 | 233.50 | 192.86577 | 5.22554 |

[a] The origin of the image *line* and *sample* coordinate system is at the center of the top left pixel, with *line* increasing downwards and *sample* to the right, when the image is displayed in its normal orientation. The spacecraft $-X$ axis points in the direction of increasing *line* and $-Z$ axis in the increasing *sample* direction.

[b] Estimated measurement uncertainties ∼0.5 pixel in line and sample.

[c] RA and DEC refer to right ascension and declination in the International Celestial Reference Frame (ICRF).

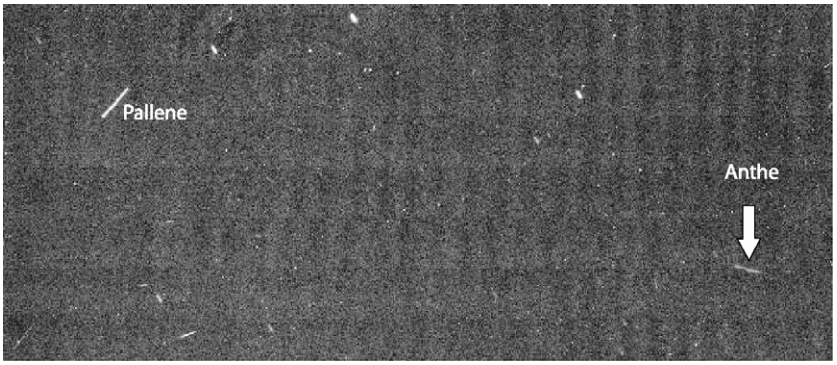


Fig. 2. Section of *Cassini* NAC image N1475699034, taken on 2004 October 5 19:56:54.839 with an exposure duration of 220 s. Due to camera motion during the long exposure, the stars appear as streaks from top-left to bottom-right in the image. Planetary satellites or cosmic rays appear as streaks in differing directions. The bright streak in the top left is Pallene. The fainter streak in the bottom right is Anthe.

confirming this as a valid detection. The relevant section of image N1475699034 is shown in Fig. 2.

### 2.4. Final observation dataset

Over the following 3 days, ending 2007 June 29, a further 21 images of Anthe were found. In total, 63 detections of Anthe were located in images taken between 2004 June 1 and 2007 June 15, representing an observation time-span of 1109 days. The final orbit solution using the full observation span had an rms uncertainty in the fitted position vector of 4.8 km. See Section 3 for further description of the orbital solutions.

The observations of Anthe are listed in Table 2, along with reduced data for each image. In addition to their image line and sample coordinates, equivalent coordinates in terms of right ascension and declination are provided. Fig. 3 shows the area distribution of the full set of observations in the equatorial plane of Saturn, based on the numerically integrated positions, using the model described in Section 3. NAC images are indicated by crosses and WAC images by triangles.

### 2.5. Size estimate

For an initial estimate of the physical size of Anthe, measurements were made relative to Pallene using the image N1475699034 in which the field of view contains trailed images of both objects (Fig. 2). Summing the pixel DN values for a 30 by 30 pixel block containing the Pallene trail gave 66,528, while an equivalent block of nearby background totalled 63,164 yielding a summed excess DN in the aperture of 3364. For Anthe, where the trail is closer to the sample axis, a block of 30 by 20 pixels containing the trail was summed and totalled 43,559 DN; background was taken from a pair of equivalent blocks just above and below giving 43,008 and 42,806 DN, a mean of 42,907: the summed excess DN in the block containing Anthe was thus 652. The ranges and phases of the two objects are similar, and in the absence of information about albedos we assume these to be comparable and thus estimate the cross sectional areas of the bodies to be in the same ratio as the fluxes: 652/3364 or ∼0.19. Lacking shape or orientation information, we then estimate the ratio of diameters to be the square root of this, namely 0.44. The listed diameter of Pallene is 4 km (Spitale et al., 2006), so this implies a diameter for Anthe of ∼1.8 km.

## 3. Orbital solutions

A planetocentric reference frame was adopted, with $x$-axis corresponding to the position of the ascending node of Saturn's equatorial plane on the Earth mean equator at the J2000 epoch (2451545.0 JED). The $z$-axis is directed along Saturn's spin axis at epoch (pointing north) and the $y$-axis is orthogonal to $x$ and $z$, following the usual right-handed system. The chosen epoch for the orbital solutions is 2454250.66883907 JED, equivalent to 2007 May 30 04:02:02.511 UTC. The key constants used in the orbit determination are given in Table 3, while Table 4 lists the SPICE kernels (Acton, 1996) used in the orbit determination and numerical modeling.

Preliminary orbital solutions were obtained using a uniformly precessing Keplerian ellipse model (Taylor, 1998), incorporating the effects of Saturn's oblateness up to terms in $J_6$, and solving for the orbital elements at the chosen epoch. However, this model only provides a 2-body picture of the dynamics. As discussed in the previous section, at the earliest possible stage in the orbit fitting process, in order to allow for the possibility of significant perturbations from other nearby satellites,

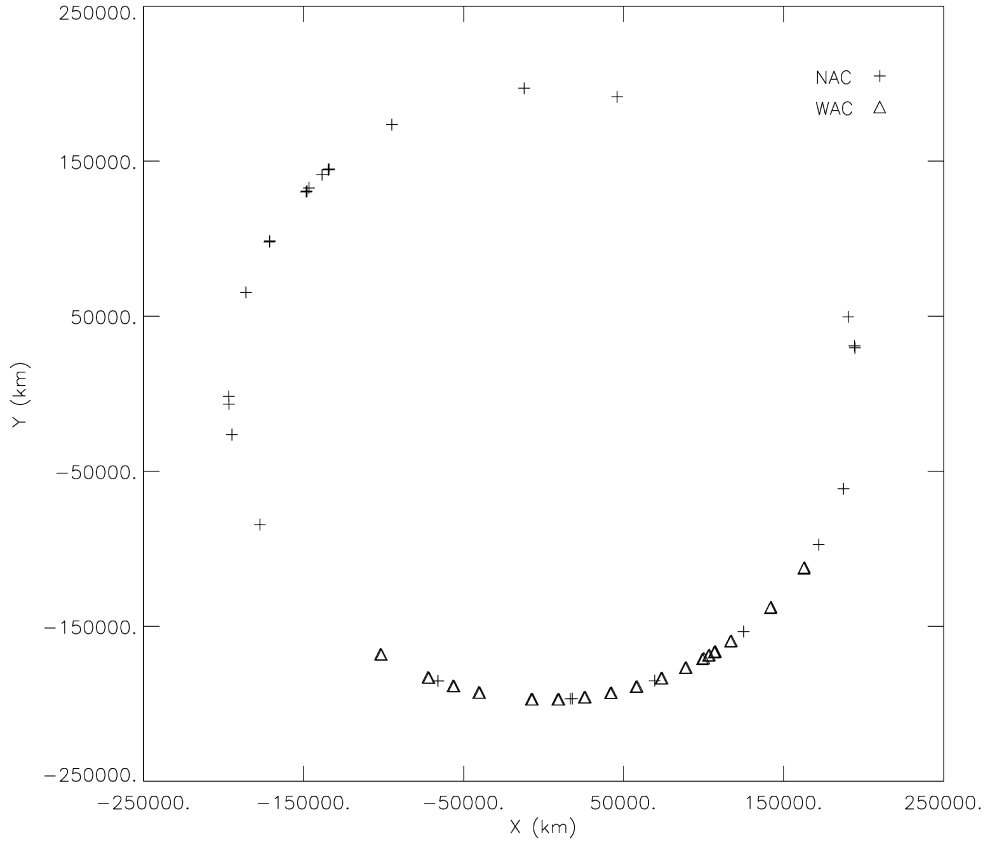


Fig. 3. Orbital coverage for *Cassini* ISS observations of Anthe, in the J2000 frame, projected on to the equatorial plane of Saturn. NAC observations are indicated by crosses and WACs by triangles.

a more sophisticated model was adopted, based on a numerical integration of the full equations of motion in three dimensions, solving for the initial state of Anthe at epoch. In this model, perturbations from the eight major satellites of Saturn (Mimas, Enceladus, Tethys, Dione, Rhea, Titan, Hyperion and Iapetus) were included, in addition to those due to Prometheus, Pandora, Janus, Epimetheus and those of Jupiter, Saturn and the Sun. The force terms resulting from the satellite, planetary and solar perturbations were calculated using position vectors extracted from the JPL ephemerides listed in Table 4. Position vectors for the perturbing bodies were rotated from the J2000 frame to the integration reference frame using the pole position for Saturn given in Table 3, obtained by precessing the pole position of Jacobson (2004) to the chosen fit epoch for this work, using rates of −0.04229 deg/cy in RA and −0.00444 deg/cy in DEC (Jacobson, 2004). The oblateness of Saturn was taken into account up to terms in $J_6$. The adopted satellite $GM$ values used in the numerical integration model are given in Table 5. A nominal $GM$ value of 0.0001 km$^3$ s$^{-2}$ was assigned to Anthe, however the results are insensitive to this value. The results were similarly insensitive to the presence of Methone and Pallene, which were therefore excluded from the fitted model (see Section 4 for further comments).

Numerical integration of both the equations of motion and the variational equations was performed using the 12th-order Runge–Kutta–Nyström RKN12(10)17M algorithm of Brankin et al. (1989). For more details relating to the numerical integration and model fitting scheme used in this work, see Murray et al. (2005).

Table 3
Saturn constants used in orbit determination and numerical modeling

| Constant | Value[a] | Units |
|---|---|---|
| Pole (RA, DEC) | (40.584275222264, 83.5369415702692) | deg |
| $GM$ | 37,931,284.0 | km$^3$ s$^{-2}$ |
| Radius, $R_s$ | 60,330 | km |
| $J_2$ | 0.016292 | |
| $J_4$ | −0.000931 | |
| $J_6$ | 0.000091 | |

[a] Pole position from Jacobson (2004), precessed to the fit epoch. Reference radius from Kliore et al. (1980). Zonal harmonics and $GM$ from Jacobson (2004).

The final solution for the state vector at epoch in the planetocentric J2000 frame, from a fit to the full time-span of observations, is given in units of km and km/s in Table 6 (if required, this may be rotated back into the integration reference frame using the Saturn pole position given in Table 3). A total of 62 observations were included in the fit. The observation from N1473631252, a long exposure 'trailed' image (exposure duration 460 s), was found to have fit residuals of 3.491 lines and −2.287 samples and has been excluded from the fit shown in Table 6. Although we believe this to be a firm detection, satisfactory image pointing could not be derived due to the trailing of star images. Fit residuals, in units of pixels,

Table 4
SPICE kernels used in orbit determination and numerical modeling

| Kernel name[a] |
|---|
| naif0008.tls |
| cas00106.tsc |
| cpck17May2007.tpc |
| cpck_rock_19Apr2007_merged.tpc |
| de405s.bsp |
| jup263.bsp |
| sat242.bsp |
| 070209AP_SCPSE_06356_08222.bsp |
| 070620AP_SCPSE_08102_10191.bsp |
| 070517AP_SCPSE_07137_07153.bsp |
| 070524BP_SCPSE_07144_07153.bsp |
| 070530AP_SCPSE_07146_07169.bsp |
| 070604AP_SCPSE_07155_07169.bsp |
| 070609AP_SCPSE_07160_07169.bsp |
| 070615AP_SCPSE_07162_07185.bsp |
| 070620AP_SCPSE_07171_07185.bsp |
| 070625AP_SCPSE_07176_07185.bsp |
| 060717AP_RE_90165_14363.bsp |
| 060222AP_IRRE_00256_14363.bsp |
| 061204AP_IRRE_04343_14363.bsp |
| 041014R_SCPSE_01066_04199.bsp |
| 041219R_SCPSE_04199_04247.bsp |
| 050105RB_SCPSE_04247_04336.bsp |
| 050214R_SCPSE_04336_05015.bsp |
| 050411R_SCPSE_05015_05034.bsp |
| 050414RB_SCPSE_05034_05060.bsp |
| 050504R_SCPSE_05060_05081.bsp |
| 050506R_SCPSE_05081_05097.bsp |
| 050513RB_SCPSE_05097_05114.bsp |
| 050606R_SCPSE_05114_05132.bsp |
| 050623R_SCPSE_05132_05150.bsp |
| 050708R_SCPSE_05150_05169.bsp |
| 050802R_SCPSE_05169_05186.bsp |
| 050825R_SCPSE_05186_05205.bsp |
| 050907R_SCPSE_05205_05225.bsp |
| 050922R_SCPSE_05225_05245.bsp |
| 051011R_SCPSE_05245_05257.bsp |
| 051021R_SCPSE_05257_05275.bsp |
| 051114R_SCPSE_05275_05293.bsp |
| 051213R_SCPSE_05293_05320.bsp |
| 060111R_SCPSE_05320_05348.bsp |
| 060213R_SCPSE_05348_06005.bsp |
| 060321R_SCPSE_06005_06036.bsp |
| 060417R_SCPSE_06036_06068.bsp |
| 060515R_SCPSE_06068_06099.bsp |
| 060614R_SCPSE_06099_06130.bsp |
| 060719R_SCPSE_06130_06162.bsp |
| 060810R_SCPSE_06162_06193.bsp |
| 060907R_SCPSE_06193_06217.bsp |
| 060925R_SCPSE_06217_06240.bsp |
| 061013R_SCPSE_06240_06260.bsp |
| 061108R_SCPSE_06260_06276.bsp |
| 061116R_SCPSE_06276_06292.bsp |
| 061129RB_SCPSE_06292_06308.bsp |
| 061213R_SCPSE_06308_06318.bsp |
| 070109R_SCPSE_06318_06332.bsp |
| 070117R_SCPSE_06332_06342.bsp |
| 070125R_SCPSE_06342_06356.bsp |
| 070208R_SCPSE_06356_07008.bsp |
| 070213R_SCPSE_07008_07023.bsp |
| 070312R_SCPSE_07023_07042.bsp |
| 070405R_SCPSE_07042_07062.bsp |
| 070430R_SCPSE_07062_07077.bsp |
| 070507R_SCPSE_07077_07094.bsp |
| 070517R_SCPSE_07094_07106.bsp |

[a] Kernels are available by anonymous ftp from ftp://naif.jpl.nasa.gov/pub/naif/CASSINI/kernels.

Table 5
$GM$ values for other perturbing bodies used in orbit determination and numerical modeling

| Body | $GM$[a] ($km^3\ s^{-2}$) |
|---|---|
| Sun | 132,712,440,044.2083 |
| Jovian system | 126,712,767.8578 |
| Prometheus | 0.01045 |
| Pandora | 0.00905 |
| Janus | 0.12758 |
| Epimetheus | 0.0354 |
| Mimas | 2.50441904258041 |
| Enceladus | 7.20596192297641 |
| Tethys | 41.2139225215060 |
| Dione | 73.1120820490921 |
| Rhea | 153.942176327879 |
| Titan | 8978.14455235218 |
| Hyperion | 0.370847384392641 |
| Iapetus | 120.5078146418220 |

[a] Values from SPICE kernels cpck17May2007.tpc and cpck_rock_19Apr2007_merged.tpc.

Table 6
Solution for the planetocentric state vector of Anthe, from a fit to *Cassini* ISS data (epoch 2007 May 30 04:02:02.511 UTC, J2000 frame)

| Anthe | | Units |
|---|---|---|
| $x$ | $0.892057695190959E+04 \pm 4.4203639968$ | km |
| $y$ | $-0.196984855354612E+06 \pm 0.1746996039$ | km |
| $z$ | $0.137069514624024E+05 \pm 1.9014415378$ | km |
| $\dot{x}$ | $0.138042908445516E+02 \pm 0.0003491170$ | $km\ s^{-1}$ |
| $\dot{y}$ | $0.525424548923838E+00 \pm 0.0000648009$ | $km\ s^{-1}$ |
| $\dot{z}$ | $-0.122840056158782E+01 \pm 0.0001163502$ | $km\ s^{-1}$ |
| rms | 0.456 (NAC) 0.281 (WAC) | pixel |
| rms | 0.563 (NAC) 3.463 (WAC) | arcsec |

(*continued in the next column*)

Table 4 (*continued*)

are displayed as a function of observation time in Fig. 4. NAC observations are shown by crosses and WACs by triangles. The overall rms fit residual is 0.456 pixel for the 27 NAC images and 0.281 pixel for the 35 WACs, equivalent to approximately 0.563 and 3.463 arcsec, respectively. Comparing with the estimated measurement error of 0.5 pixel, we see that the NAC rms residual is of a similar order, while the WAC rms is smaller by approximately a factor of 2. Overall, this suggests that any systematic errors in the modeled orbit are small. The final rms uncertainty in the fitted position vector, in the frame of the integration, was 4.8 km. We discuss the uncertainties further in Section 5.

Table 7 provides planetocentric orbital elements, $a_{\rm calc}$, $e$, $i$, $\Omega$, $\varpi$, $\lambda_0$ and $n$, corresponding to semi-major axis, eccentricity, inclination, longitude of ascending node, longitude of pericenter, mean longitude and mean motion. These were generated by fitting a uniformly precessing ellipse model to the numerically

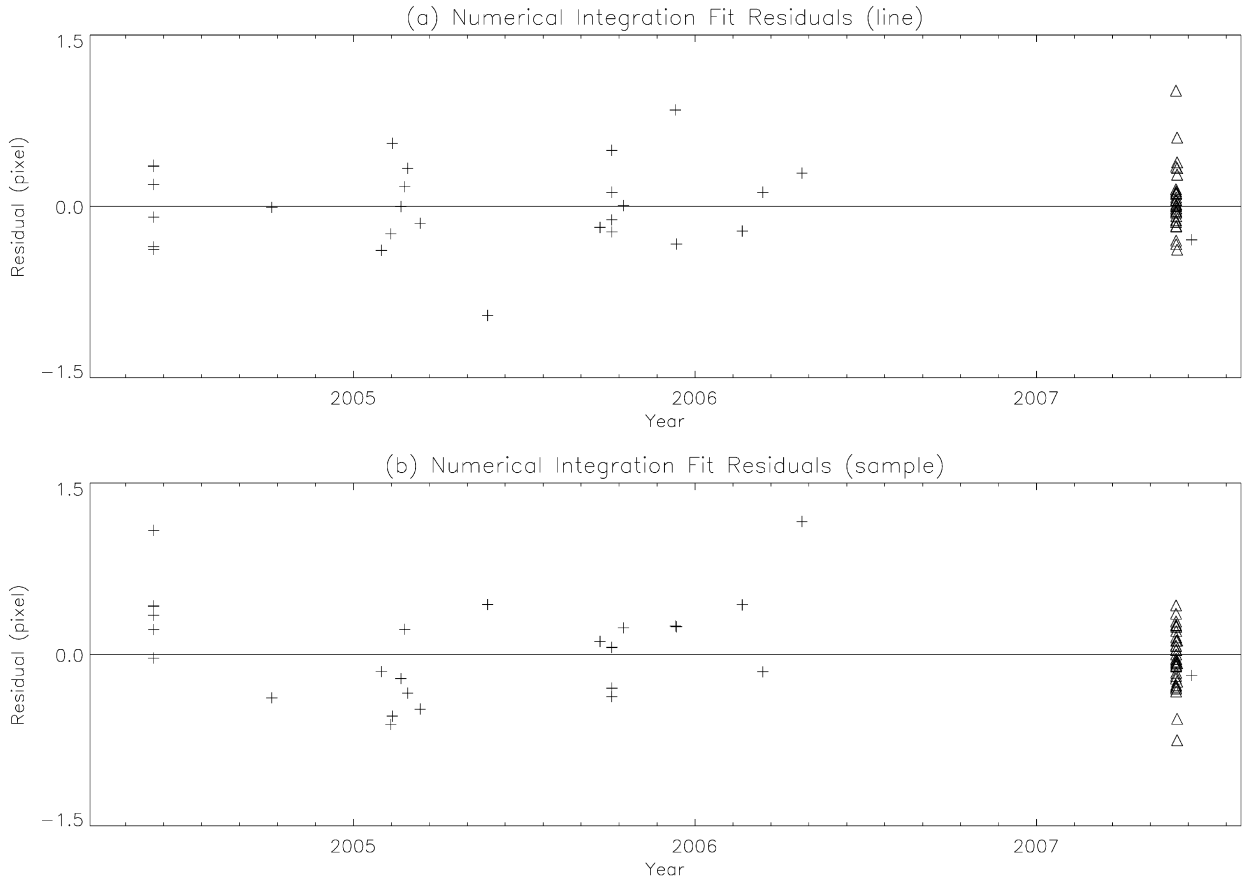


Fig. 4. Numerical integration fit residuals as a function of time: (a) *line* direction, (b) *sample* direction. Units are pixels. NAC observations are indicated by crosses and WACs by triangles.

Table 7
Planetocentric orbital elements

| Parameter[a] | Fitted value | Units |
|---|---|---|
| Fit epoch (UTC) | 2007 May 30 04:02:02.511 | UTC |
| Semi-major axis, $a_{\rm calc}$ | $197{,}668.545 \pm 0.008$ | km |
| Eccentricity, $e$ | $0.0010223 \pm 0.00000006$ | |
| Inclination, $i$ | $0.159 \pm 0.003$ | deg |
| Longitude of ascending node, $\Omega$ | $5 \pm 1$ | deg |
| Longitude of pericenter, $\varpi$ | $53.422 \pm 0.003$ | deg |
| Mean longitude, $\lambda$ | $141.715119 \pm 0.000008$ | deg |
| Mean motion, $n$ | $347.31687 \pm 0.00002$ | deg/day |
| Pericenter rate, $\dot{\varpi}_{\rm calc}$ | 0.80042737 | deg/day |
| Nodal rate, $\dot{\Omega}_{\rm calc}$ | −0.79858779 | deg/day |
| **Parameter** | **Mean value ± libration** | **Units** |
| Semi-major axis, $a_{\rm mean}$ | $197{,}655 \pm 26$ | km |
| Eccentricity, $e_{\rm mean}$ | $0.0012 \pm 0.0008$ | |
| Inclination, $i_{\rm mean}$ | $0.017 \pm 0.004$ | deg |
| Libration period, $a_{\rm mean}$ | 913 | days |
| Libration period, $e_{\rm mean}$ and $i_{\rm mean}$ | 1826 | days |

[a] All longitudes measured directly from ascending node of Saturn's equator at epoch on the Earth mean equator at J2000. Inclination measured relative to Saturn's equatorial plane at epoch. Quoted uncertainties are formal $1\sigma$ values from the fit. Mean values and their librations were obtained from a 10-year numerical integration, taking into account the resonant behavior. See Section 3 for further comments regarding the fitted inclination.

integrated orbit of Anthe over a one-day time-span, using a fine grid of regularly-spaced position vectors. The position vectors (effectively 'synthetic observations') were extracted from the numerically integrated orbit at 5 min intervals. Given the fitted value of $n$, the calculated semi-major axis, $a_{\rm calc}$, was obtained by solving the standard expression for the sidereal mean motion, $n$, in terms of the primary body radius and the zonal harmonics, up to $J_6$ (Nicholson and Porco, 1988). It should be

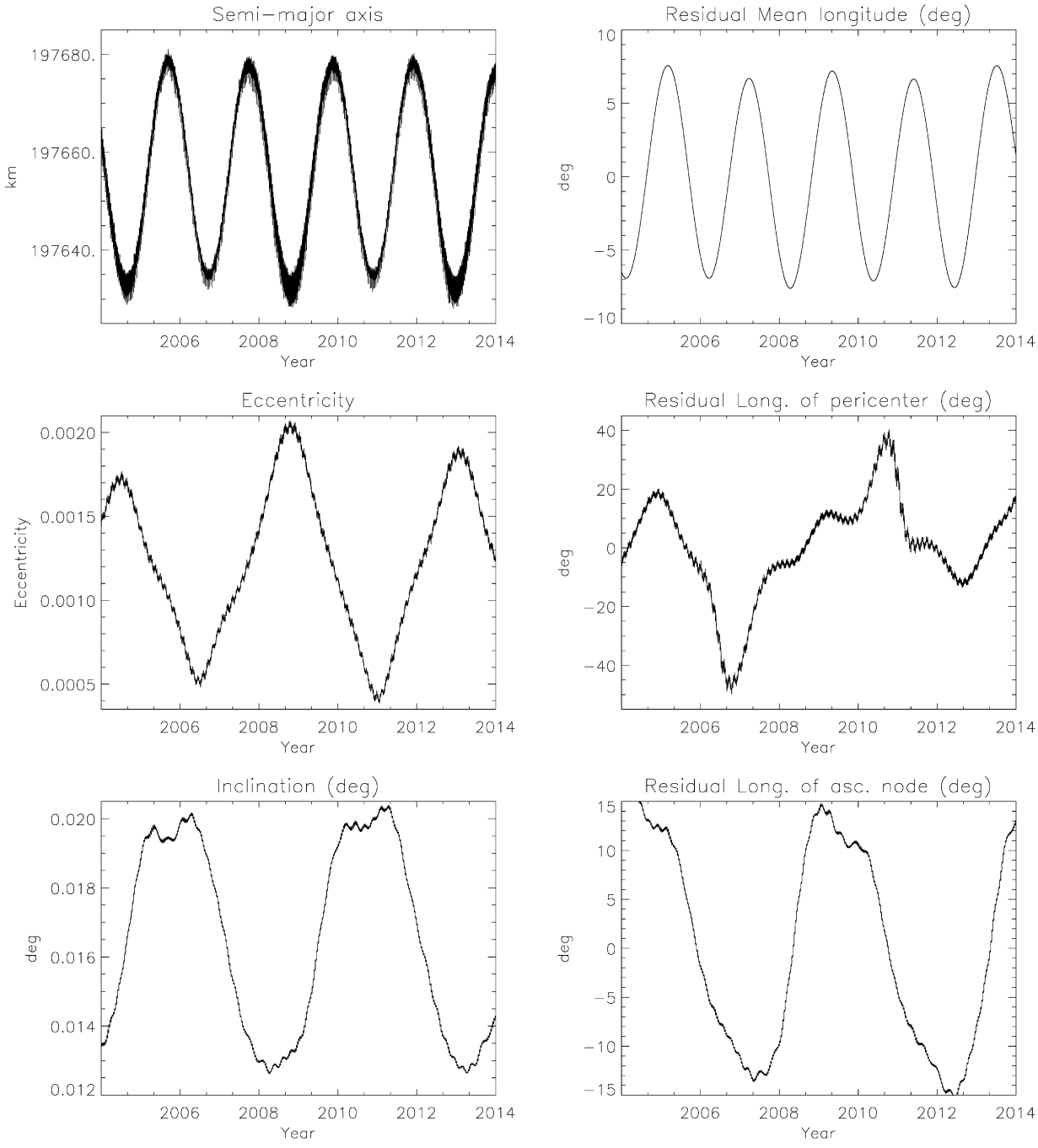


Fig. 5. Geometric orbital elements between 2004 Jan 1 and 2014 Jan 1 derived from the numerical integration, including perturbations from the 8 major satellites of Saturn plus Prometheus, Pandora, Janus and Epimetheus. Best-fit linear background trends have been subtracted from all longitude profiles. See Section 3 for further comments.

emphasized that the fitted elements in Table 7 represent a snapshot of the orbit at the time epoch of the fit, equivalent to 2007 May 30 04:02:02.511 UTC. We show in the next section that the orbital elements exhibit significant sinusoidal variation as a function of time due to a resonant perturbation from Mimas (Fig. 5). A uniformly precessing ellipse will therefore provide a poor approximation to the orbit over a time-span of more than a few days. In particular, the numerical integration results show that the resonant effect causes the semi-major axis to vary by ±26 km around a mean value of ∼197,655 km over a 913-day period. The eccentricity varies by ±0.0008 around a mean value of ∼0.0012 over a 1826-day period, and the inclination by 0.004 degrees around a mean value of ∼0.017 degrees over the same period. The estimated mean values for $a$, $e$ and $i$, taking into account the effect of the resonant behavior are therefore also provided in Table 7. Note that the fitted inclination in Table 7, $0.159 \pm 0.003$ degrees is anomalous, lying well outside the integration range given above. This anomaly is a reflection of the large uncertainty in determining the node from a precessing ellipse fit: the uncertainty in the longitude of ascending node

is ±1 degree, 3 orders of magnitude larger than the uncertainty in the fitted longitude of pericenter and 6 orders of magnitude larger than the uncertainty in the fitted mean longitude. The mean value of the inclination is thus more representative. The large uncertainty in the fitted inclination may simply reflect the breakdown of the precessing ellipse model in the presence of resonances, which in this case include inclination-type resonances.

## 4. Short-term dynamical evolution

The orbital evolution of Anthe was analyzed using the model described in the previous section, based on a numerical solution of the full equations of motion, including perturbations from the eight major satellites of Saturn, and incorporating the effects of Saturn's oblateness up to terms in $J_6$. Using this model, the initial state for Anthe from Table 6 was integrated from 2004 January 1 to 2014 January 1. State vectors for Anthe were generated at 0.15-day intervals and converted to geometric orbital elements using the method of Borderies and Longaretti (1994), Renner (2004). Unlike conventional osculating elements, these geometric elements are not contaminated by the short-period terms caused by planetary oblateness. The geometric elements are displayed as functions of time in Fig. 5. The mean longitude, longitude of pericenter and longitude of ascending node represent the residual values after linear background trends have been subtracted from each. Constant values have also been subtracted from the longitudes in order to give approximately zero mean variability. The subtracted background trends correspond to angular rates in degrees/day of 347.349, 0.78982209 and −0.79858779, respectively, for the mean longitude, longitude of pericenter and longitude of ascending node. The subtracted constant background values were 24.811303, 169.49722 and 193.51327 degrees, respectively.

The clear oscillatory component shown by the orbital elements in Fig. 5 is the effect of a mean motion resonance. From an analysis of the orbital elements, we estimate the mean semi-major axis of Anthe to be 197,654.61 km, with a sinusoidal variation of ±25.50 km over a period of approximately 913 days. The mean longitude varies with the same period. The periods for the variations in eccentricity and inclination are in both cases 1826 days; double the period for the semi-major axis and mean longitude. In Fig. 6, we show the behavior of the orbital elements derived from a simulation where Mimas has been excluded from the numerical model. The variations described above have disappeared, demonstrating that the dominant resonant perturbation comes from Mimas. Removing Tethys from the simulation, but including Mimas, showed that any possible modulating effect from the Mimas–Tethys 4:2 resonance is insignificant over the 10-year time-span studied.

In order to identify the resonant argument concerned, a numerical search for all significant mean motion resonances close to the mean semi-major axis of Anthe, originating from any of the inner or major outer satellites of Saturn, was conducted. Using the standard definition of exact resonance which requires the time-derivative of the resonant argument to be zero (Murray and Dermott, 1999), the procedure involved iteratively solving for the semi-major axis which zeros the time-derivative, given the semi-major axis of the perturbing body and the pericenter and node rates. The 11:10 outer resonance with Mimas was identified as a possible candidate.

There are 14 valid arguments in the expansion of the disturbing function to fourth degree in the eccentricities and inclinations of the form $\phi = 11\lambda' - 10\lambda$. Two of these arguments were calculated to have equivalent semi-major axes less than 1.37 km away from the estimated mean semi-major axis of Anthe (197,654.61 km), namely: $\phi_1 = 11\lambda' - 10\lambda - \varpi$ at 197,655.98 km and $\phi_2 = 11\lambda' - 10\lambda - \varpi' - \Omega' + \Omega$ located at 197,655.11 km.

The temporal behavior of all 14 resonant arguments was examined by numerically integrating the orbits of the 8 major saturnian satellites, in addition to Anthe, over a one hundred-year period from 2004 January 1. Starting conditions for the major satellites came from the latest JPL spice kernels (Table 4), while Anthe's orbit used the solution given in Table 6. Results showed that, of the 14 arguments in question, the two described in the previous paragraph are librating. The others are circulating. In Figs. 7a and 7b, we show the time-evolution of the two resonant arguments in question, $\phi_1 = 11\lambda' - 10\lambda - \varpi$ and $\phi_2 = 11\lambda' - 10\lambda - \varpi' - \Omega' + \Omega$, between the years 2004 and 2054. We see that both arguments are indeed librating, confirming that Anthe is located within this resonance. From the Fourier spectra of the resonant arguments, Fig. 7c, we estimate the dominant period of libration to be 761 days.

Second-order inclination-type resonances of the form $\phi = 22\lambda' - 20\lambda$ between Mimas and Anthe were also examined; however, these resonance were found to be located too far from the estimated mean semi-major axis of Anthe to be of significance. We would anyway expect the effects of such resonances, in general, to be weaker than those of their first-order counterparts.

In addition to the first-order resonances between Mimas and Anthe described above, the search revealed a second-order mean motion resonant relationship between Methone and Anthe of the form $\phi = 77\lambda' - 75\lambda$, where the primed quantity refers to Anthe. Eccentricity-type resonances of this form, with arguments $\phi = 77\lambda' - 75\lambda - 2\varpi$, $\phi = 77\lambda' - 75\lambda - 2\varpi'$ and $\phi = 77\lambda' - 75\lambda - \varpi - \varpi'$, were found to be located within 1 km of the semi-major axis of Anthe, using the value 194,230 km for the semi-major axis of Methone from Jacobson et al. (2007). Though the addition of the resonant perturbation between Methone and Anthe has no significant effect on the residuals in the fit, reducing them by only 0.01 pixel, a factor of 10 smaller than the pointing uncertainties, the proximity of Anthe to the 77:75 eccentricity-type resonances with Methone suggests that Anthe may in fact be perturbed by Methone. Since Methone is also itself in a resonance with Mimas (Spitale et al., 2006), there is an additional indirect interaction between Methone and Anthe via Mimas. However, a long-term numerical integration including Methone, using a nominal $GM$ value of 0.001 $\mathrm{km}^3\,\mathrm{s}^{-2}$ for Methone, confirmed that the first-order

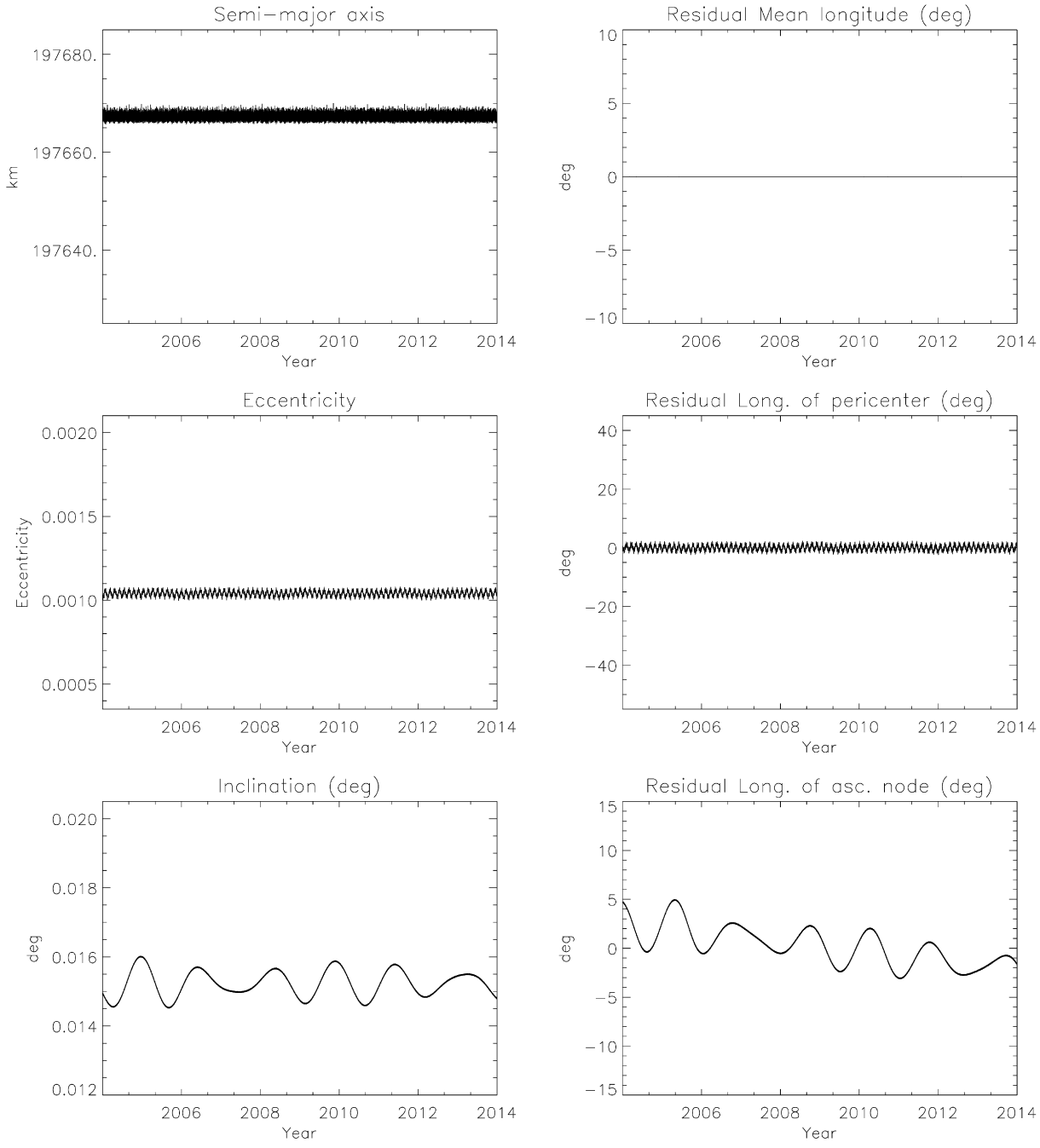


Fig. 6. As Fig. 5 except Mimas has been excluded from the model.

Mimas–Anthe resonances dominate the dynamics of Anthe and that any Methone effect, whether direct or indirect, is insignificant.

## 5. *GM* value for Mimas

The resonant perturbation of Anthe by its much larger and more massive near-neighbor, Mimas, ensures that the motion of Anthe is highly sensitive to the mass of Mimas. We exploit this in order to estimate the $GM$ value of Mimas (where $G$ is the universal gravitational constant and $M$ is the mass of Mimas). Jacobson et al. (2006) were able to improve the previous best estimate of the $GM$ of Mimas by a factor of 5 by analyzing the libration between Methone and Mimas. Here we adopt a similar approach, in this case estimating the $GM$ of Mimas by analyzing the libration between Anthe and Mimas.

A numerical integration of the full equations of motion was fitted to *Cassini* ISS observations of both Mimas and Anthe, solving simultaneously for the states at epoch of Mimas and Anthe and for the $GM$ value of Mimas. Included in the model were the perturbing effects from the other 7 major satellites of Saturn (Enceladus, Tethys, Dione, Rhea, Titan, Hyperion and Iapetus), in addition to those from Prometheus, Pandora, Janus,

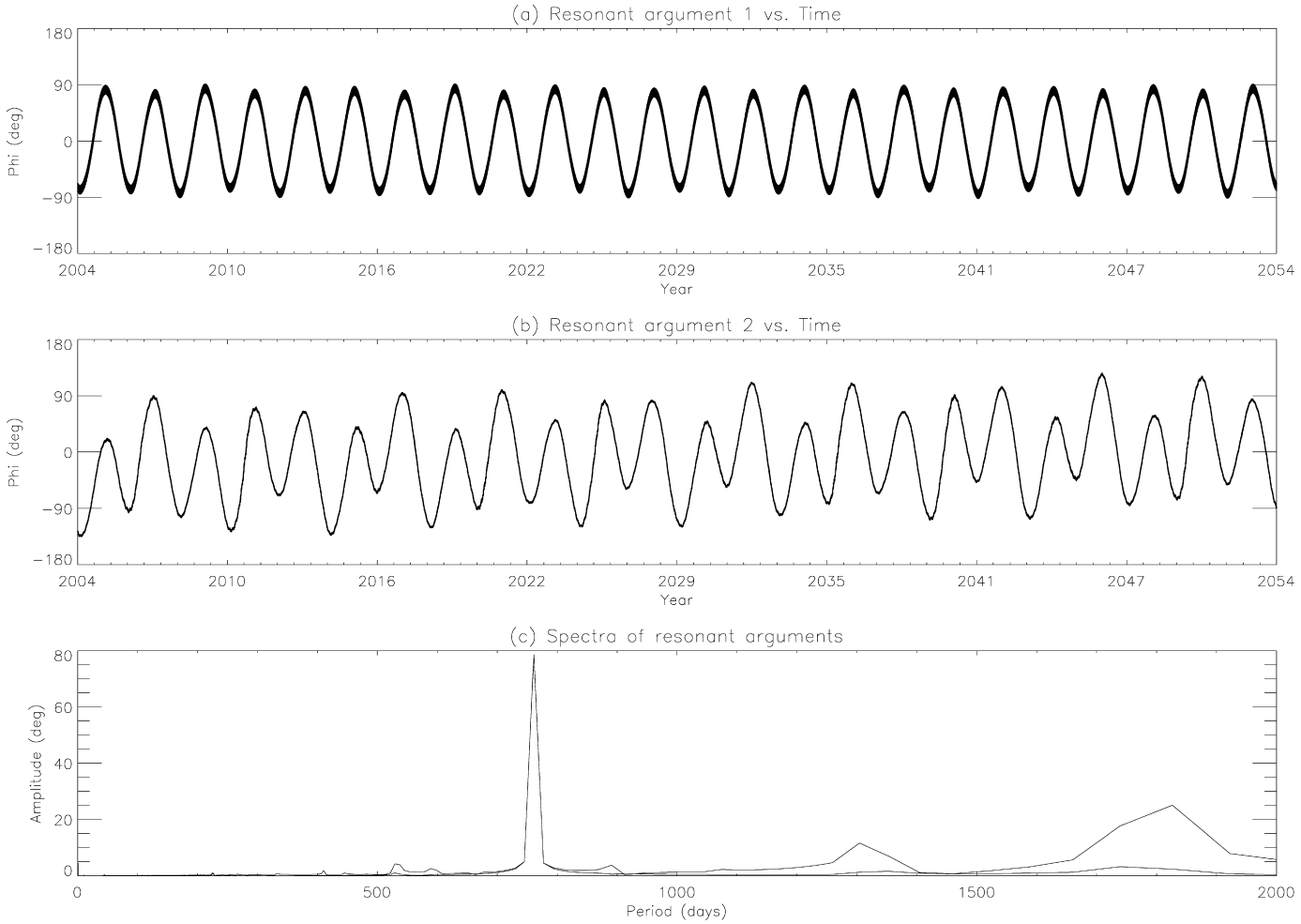


Fig. 7. Behavior of resonant arguments as a function of time, from numerical integration. (a) Resonant argument $\phi_1 = 11\lambda' - 10\lambda - \varpi$ versus time. (b) Resonant argument $\phi_2 = 11\lambda' - 10\lambda - \varpi' - \Omega' + \Omega$ versus time. (c) Fourier spectra of (a) and (b) plotted on the same axes, showing a dominant period of 761 days and amplitude 78 degrees. The two spectra in (c) are indistinguishable in the region of the strong peak, using this display scale.

and Epimetheus. As before, the effect of Saturn's oblateness was included up to terms in J6, along with the perturbations from Jupiter and the Sun. Position vectors for the perturbing bodies at each integration time-step were obtained from the latest JPL ephemerides via SPICE kernels (Table 4), as were the initial state at epoch and initial $GM$ for Mimas.

This model was fitted to the 62 *Cassini* ISS observations of Anthe used previously, together with 44 *Cassini* ISS observations of Mimas, spanning a total of 3 years and 18 days. A converged fit was obtained, with rms residuals for the NAC and WAC images of 1.908 and 0.329 pixel.

Our solution for the $GM$ value of Mimas is $2.509 \pm 0.004$ km$^3$ s$^{-2}$. By comparison, Jacobson et al. (2006) obtained the value $2.504 \pm 0.002$ km$^3$ s$^{-2}$ from a fit to observations of Mimas, Tethys and Methone.

## 6. Discussion

Following the earlier discoveries of Methone and Pallene, also by the *Cassini* ISS Team (Spitale et al., 2006), Anthe is the third new satellite to be found orbiting in the region between Mimas and Enceladus. Dynamically, the possibility exists that these three satellites collectively form part of a larger family of small moons, the other members of which are yet to be discovered. Burns (private communication) has suggested that a possible G-ring parent body may also be a member of such a family.

Roussos et al. (2006) reported on the probable detection of a ring arc (R/2006 S 5) close to the orbit of Methone, on the basis of two electron depletion signals recorded using the *Cassini* LEMMS (Low Energy Magnetospheric Measurements System). They estimated equivalent equatorial distances for these signals of 197,700 and 194,700 km, respectively. It is notable that the first of these signals is close to the mean semi-major axis of Anthe (197,655 km).

Spitale et al. (2006) discussed the possibility that an object originally seen in a single *Voyager* 2 image and given the designation S/1981 S 14 (Synnott, 1986) could be either Methone or Pallene. Synnott (1986) had originally estimated a radial distance of about 210,000 km, while Gordon et al. (1996), referring to the object as Candidate D in their Table IV, re-estimated the radial distance to be 197,620 km. The large disagreement

in the estimates is an indication of the difficulty encountered in deriving pointing corrections for this image. Following a reworking of the pointing, Spitale et al. (2006) concluded that S/1981 S 14 is Pallene and successfully included it in their orbital solution for Pallene, with fit a residual of 0.6 pixel. Although the work of both Gordon et al. (1996) and Spitale et al. (2006) pre-dates the discovery of Anthe, it is interesting to note that the Gordon et al. (1996) estimate of the radial distance for S/1981 S 14 was actually within 35 km of the mean semi-major axis of Anthe. However, the conclusion of Spitale et al. (2006) that S/1981 S 14 is Pallene, suggests that this is no more than an interesting coincidence.

Our estimate of the $GM$ of Mimas of $2.509 \pm 0.004\ \mathrm{km}^3\ \mathrm{s}^{-2}$, determined by fitting observations of Mimas and Anthe is consistent with Jacobson et al. (2006), who obtained the value $2.504 \pm 0.002\ \mathrm{km}^3\ \mathrm{s}^{-2}$ by fitting observations of Mimas, Tethys and Methone. Mimas and Tethys are themselves in a 4:2 inclination type resonance and the further constraint provided by the addition of Tethys observations to the fit may explain the better precision of the Jacobson et al. (2006) estimate. It may also account for the larger NAC rms of 1.908 pixel obtained for the mass estimate in the current work compared to the estimated measurement uncertainty of 0.5 pixel. On the other hand, the fact that such a precise estimate has been possible by modeling the Mimas–Anthe effect alone again confirms that the influence of Tethys is relatively insignificant. The Mimas–Tethys resonant argument has a period of approximately 72 years and it was not within the scope of this work to incorporate a span of historical observations sufficient to resolve this effect. The obvious next step would be to fit simultaneously observations of Mimas, Tethys and Methone, together with the new satellite, Anthe, solving for the masses of Mimas and Tethys. This may possibly improve the precision in the mass estimates for Mimas and Tethys still further.

The possible existence of a resonant interaction between Anthe and Methone suggests that, in principle, it may be possible to estimate their masses using a similar method to that used to estimate the mass of Mimas, described earlier. However, as indicated previously, the effects of this second-order resonance are currently not detectable.

In conclusion, it is now becoming clear that the known resonant interactions between Mimas and Tethys on the one hand, and Enceladus and Dione on the other, are in fact only part of a much more complex and beautiful web of resonant interactions that encompass the newly discovered satellites Anthe, Methone, Pallene and possibly some satellites yet to be discovered. The origin and evolution of these resonances will benefit from further detailed study.

## Acknowledgments

The authors thank the members and associates of the *Cassini* ISS team. N.C., C.M., M.E. and K.B. also acknowledge the financial support of the UK Science and Technology Facilities Council. Part of this work was carried out at the Jet Propulsion Laboratory, California Institute of Technology, under a contract with the National Aeronautics and Space Administration. The staff members at the Cassini Imaging Central Laboratory for Operations (CICLOPS) are acknowledged for the sequencing of the imaging observations used in this analysis. C.P. acknowledges funding by NASA/JPL and the *Cassini* Project. Finally, the authors thank the two anonymous referees for their valuable comments and suggestions.

## References

Acton, C.H., 1996. Ancillary data services of NASA's navigation and ancillary information facility. Planet. Space Sci. 44, 65–70.

Brankin, R.W., Gladwell, I., Dormand, J.R., Prince, P.J., Seward, W.L., 1989. A Runge–Kutta–Nystrom code. ACM Trans. Math. Software 15 (1), 31–40.

Borderies, N., Longaretti, P.-Y., 1994. Test particle motion around an oblate planet. Icarus 107, 129–141.

Cooke, M.L., 1991. Saturn's rings: Radial variation in the Keeler Gap and C ring photometry. Ph.D. thesis, Cornell University.

Gordon, M.K., Murray, C.D., Beurle, K., 1996. Further evidence for the existence of additional small satellites of Saturn. Icarus 121, 114–125.

Jacobson, R.A., 2004. The orbits of the major saturnian satellites and the gravity field of Saturn from spacecraft and Earth-based observations. Astron. J. 128, 492–501.

Jacobson, R.A., Spitale, J., Porco, C.C., Owen, W.M., 2006. The $GM$ values of Mimas and Tethys and the libration of Methone. Astron. J. 132, 711–713.

Jacobson, R.A., Spitale, J., Porco, C.C., Beurle, K., Cooper, N.J., Evans, M.W., Murray, C.D., 2007. Revised orbits of Saturn's small inner satellites. Astron. J. 135, 261–263.

Kliore, A.J., Patel, I.R., Lindal, G.F., Sweetham, D.N., Hotz, H.B., Waite Jr., J.H., McDonough, T.R., 1980. Structure of the ionosphere and atmosphere of Saturn from Pioneer 11 radio occultation. J. Geophys. Res. 85, 5857–5870.

Murray, C.D., Dermott, S.F., 1999. Solar System Dynamics. Cambridge Univ. Press, Cambridge, UK.

Murray, C.D., Cooper, N.J., Evans, M.W., Beurle, K., 2005. S/2004 S 5: A new co-orbital companion for Dione. Icarus 179, 222–234.

Nicholson, P.D., Porco, C.C., 1988. A new constraint on Saturn's zonal gravity harmonics from Voyager observations of an eccentric ringlet. J. Geophys. Res. 93 (B9), 10209–10224.

Porco, C.C., and the Cassini Imaging Team, 2004a. S/2004 S 1 and S/2004 S 2. IAU Circ. 8389.

Porco, C.C., and the Cassini Imaging Team, 2004b. Satellites and rings of Saturn. IAU Circ. 8432.

Porco, C.C., and 24 colleagues, 2005a. Cassini Imaging Science: Initial results on Saturn's rings and small satellites. Science 307, 1226–1236.

Porco, C.C., and the Cassini Imaging Team, 2005b. S/2005 S 1. IAU Circ. 8524.

Porco, C.C., and the Cassini Imaging Team, 2007. S/2007 S 4. IAU Circ. 8557.

Renner, S., 2004. Dynamique des anneaux et des satellites planetaires: Application aux arcs de Neptune et au systeme Promethee–Pandore. Ph.D. thesis, L'Observatoire de Paris.

Roussos, E., Jones, G.H., Krupp, N., 2006. R/2006 S 5. IAU Circ. 8773.

Sheppard, S.S., Jewitt, D.C., Kleyna, J., 2007. S/2007 S 1, S/2007 S 2 and S/2007 S 3. IAU Circ. 8836.

Spitale, J.N., Jacobson, R.A., Porco, C.C., Owen, W.M., 2006. The orbits of Saturn's small satellites derived from combined historic and Cassini Imaging observations. Astron. J. 132, 692–710.

Stetson, P.B., 1987. DAOPHOT—A composite program for crowded-field stellar photometry. Publ. Astron. Soc. Pacific 99, 191–222.

Synnott, S.P., 1986. Evidence for the existence of additional small satellites of Saturn. Icarus 67, 189–204.

Taylor, D.B., 1998. Determination of starting conditions for ephemerides of the uranian satellites I–V. Nautical Almanac Office Tech. Note No. 72. http://www.hmnao.com.